Geophys. J. Int. (2000) **143,** 427–437

Colliding cascades model for earthquake prediction

Andrei Gabrielov,[1,2] Ilya Zaliapin,[3] William I. Newman[4,5,6] and Vladimir I. Keilis-Borok[3,4,7]

[1] *Department of Mathematics, Purdue University, West Lafayette,* IN 47907-1395, *USA*
[2] *Department of Earth and Atmospheric Sciences, Purdue University, West Lafayette,* IN 47907-1395, *USA*
[3] *International Institute of Earthquake Prediction Theory and Mathematical Geophysics, Russian Academy of Sciences, Moscow, Russia*
[4] *Department of Earth and Space Sciences, University of California, Los Angeles,* CA 90095-1567, *USA. E-mail: newman@ess.ucla.edu*
[5] *Department of Physics and Astronomy, University of California, Los Angeles,* CA 90095-1547, *USA*
[6] *Department of Mathematics, University of California, Los Angeles,* CA 90095-1555, *USA*
[7] *Institute of Geophysics and Planetary Physics, University of California, Los Angeles,* CA 90095-1567, *USA*

Accepted 2000 May 30. Received 2000 April 7; in original form 1999 December 22

SUMMARY

A wide set of premonitory seismicity patterns is reproduced on a numerical model of seismicity, and their performance in the prediction of major model earthquakes is evaluated. Seismicity is generated by the *colliding cascades model*, recently developed by the authors. The model has a hierarchical structure. It describes the interaction of two cascades: a *direct cascade of loading*, which is applied to the top (largest) element and transfers down the hierarchy, and an *inverse cascade of failures*, which goes up the hierarchy, from the smaller to the larger elements. These cascades collide and interact: loading leads to failures, while failures release and redistribute the loading. Three basic types of earthquake precursors are considered: (i) the clustering of earthquakes in space and time, (ii) the intensity of earthquake sequences, and (iii) the correlation distance between earthquakes. Patterns of the first two types are used in intermediate-term earthquake prediction algorithms. Patterns of the third type are found in the colliding cascades model, although they were hypothesized previously. They have not been validated by observations. For each precursor, we explore what is called an 'error diagram' showing the total duration of alarms, the rate of failures to predict, and the rate of false alarms.

Key words: aftershocks, earthquake prediction, foreshocks, seismic modelling, synthetic earthquake catalogues.

1 INTRODUCTION

1.1 The model

We explore here the process wherein seismicity undergoes a qualitative change, culminating in a major earthquake. This is done for synthetic seismicity generated by the model of colliding cascades (CC model), which is described in the Appendices. The concept of cascades has been employed in physics for more than half a century.

Originating in the context of fully developed isotropic turbulence, the original work of Kolmogoroff (Kolmogoroff 1941a,b; Batchelor 1959; Tennekes & Lumley 1972) was based on a direct cascade that would deliver energy from the largest size scales (production range) through the intervening size scales (inertial range) to the smallest size scales (dissipation range). In 2-D hydrodynamic problems, as well as in magnetohydrodynamic problems (Kraichnan & Montgomery 1980), it became apparent that cascades could emerge in the opposite direction; that is, energy could be transferred from the smallest scales through the intermediate scales to the largest scales of the system. This may be regarded, loosely, as a form of self-organization. In turbulent environments, cascades were often considered as a description of a steady process of energy transfer.

Cascades, however, are not limited conceptually to fluid problems and can occur with the deposition of energy into one size scale that then results in energy transfer to the smallest or, alternatively, the largest scales (Barenblatt 1982). In solid mechanics, particularly in the brittle stress regime, microcracking spontaneously occurs. The microscopic cracks tend to coalesce with each other to form larger cracks, which then coalesce to form still larger cracks and so on, ultimately resulting in the catastrophic failure of the system (Newman & Knopoff 1982, 1983, 1989; Allègre *et al.* 1982). The concept of cascades has

been extended to seismicity (Knopoff & Newman 1983), forest fires (Malamud *et al.* 1998; Turcotte *et al.* 1999) and other forms of clustering (Gabrielov *et al.* 1999). The colliding cascades model was first proposed by Gabrielov *et al.* (2000) in order to synthesize the three following basic features of many complex systems, not seismicity alone.

(1) *Hierarchical structure.* We consider the case of a ternary tree (Fig. 1).

(2) *Direct cascade of loading* by external sources. The load is applied at the top (largest) element and transfers down the hierarchy, thus forming a direct cascade.

(3) *Inverse cascade of failures.* The elements fail under the load. The failures start at the bottom level and expand up the hierarchy, thus forming an inverse cascade. Eventually the failures heal, ensuring a continuous functioning of the system. The direct and inverse cascades collide and interact—loading leads to failures, while failures release and redistribute the loading.

A brief description of the CC model is given in the Appendices. This model is akin to other lattice models of seismicity such as the pioneering slider-blocks model (Burridge & Knopoff 1967), the 'scaling of fracture tectonics' renormalization model (Allègre *et al.* 1982), the hierarchical model of defect development (Narkunskaya & Shnirman 1990; Shnirman & Blanter 1999), fibre bundles (Newman *et al.* 1995) and forest fires (Drossel & Schwabl 1992; Bak *et al.* 1992; Malamud *et al.* 1998; Turcotte *et al.* 1999; Gabrielov *et al.* 1999). Models of that kind are reviewed in Newman *et al.* (1994) and Turcotte (1997). They depict mainly inverse cascades, while the CC model deals with the interaction of both inverse and direct cascades. A similar approach was employed by Blanter *et al.* (1999) in modelling a magnetic dynamo. Lattice models, notwithstanding their simple design, do reproduce and explain many basic features of real seismicity, although evidently not all of them. These models do not consider directly the geometry of the fault system nor the specific physical mechanisms controlling stress and strength in the lithosphere. At best, such factors may be reflected in the parameters of a lattice model. On the other hand, lattice models reproduce common features of a wide class of chaotic processes, seismicity being just one of them.

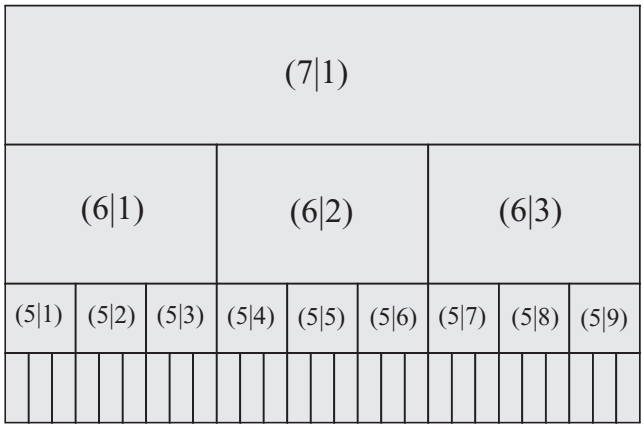

Figure 1. Structure of the three-branched or ternary tree model. The figure shows the four highest levels of the seven-level tree, which were used in the simulation. Indexing of elements is shown in brackets.

1.2 The goal

The general objective of the colliding cascades model has been to reproduce the major known features of seismicity as well as to find new premonitory phenomena, which then may be validated by the analysis of real seismicity and used for earthquake prediction. An example of seismicity generated by this model is shown in the top panel of Fig. 2. About half of the time, the sequence shown is quasi-periodic, consisting of easily identifiable cycles, with each culminating in a major event. During the remaining period, there is no clear periodicity or separation into regular cycles. Gabrielov *et al.* (2000) demonstrated that seismicity generated by the CC model exhibits basic regularities, observed in nature, including the seismic cycle, intermittency of the seismic regime, power law energy–frequency distribution, spatio-temporal clustering and a set of seismicity patterns premonitory to a strong earthquake. However, in the CC model, only the *existence* in a statistical sense has been established for premonitory patterns—it was demonstrated that on average these patterns emerge more frequently as a strong earthquake approaches. Here we examine their *performance* for predicting strong earthquakes, one by one.

The problem of earthquake prediction is posed as the consecutive stage-by-stage reduction of the time interval and spatial region where a strong earthquake might occur (Keilis-Borok 1996). It is realistically expected that prediction errors are possible. Both types of errors—false alarms and failures to predict—are illustrated in Fig. 3. (The absence of an alarm implies that no event is expected.) The choice of safety measures undertaken in response to a prediction depends on the probability of an error of each kind (Molchan 1990). Note that many important safety measures do not require a particularly low probability of an error.

Usually, the following stages of prediction are distinguished, with characteristic time intervals indicated in brackets: long term (10^1 yr), intermediate term ($10^0 - 10^{-1}$ yr), short term (10^{-2} yr), and immediate (10^{-3} yr or less). The point of departure in this study is the intermediate-term prediction based on premonitory seismicity patterns. So far this is the only kind of prediction for which statistical significance is rigorously established by worldwide tests (Molchan *et al.* 1990; Kossobokov *et al.* 1999; Vorobieva 1999).

2 GENERAL SCHEME OF PREDICTION

In the analysis of model seismicity, we follow here the general scheme of algorithmic prediction described in Keilis-Borok (1996, 1999) and Gabrielov *et al.* (1986).

2.1 Earthquake sequence

Prediction is based on the analysis of an earthquake sequence, with aftershocks excluded. A procedure for identifying main shocks and aftershocks is described in e.g. Keilis-Borok *et al.* (1980). However, the number of immediate aftershocks is retained for each main shock for further processing. As in the analysis of observations, the immediate foreshocks, which are relatively rare, are not differentiated from main shocks. An earthquake sequence is represented as

$$\{t_k, m_k, g_k, B(t_k|s)\}, \quad k = 1, 2, \ldots; \quad t_k \le t_{k+1}. \tag{1}$$

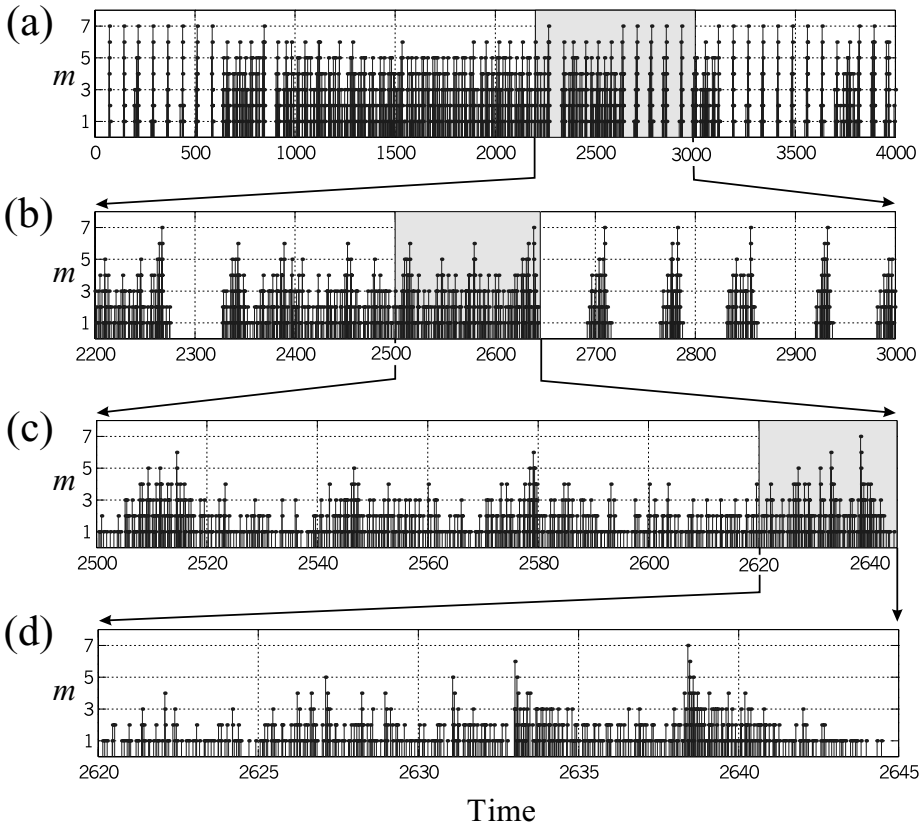

Figure 2. Synthetic earthquake sequence. The complete sequence is shown on the top panel followed by enlarged views in the following three panels.

Here t_k is the time of the kth main shock, m_k is its magnitude, g_k are the coordinates of the hypocentre and $B(t_k|s)$ is the number of aftershocks within the first s time units that reside in the interval $[t_k,\ t_k+s]$.

We single out in this sequence the 'major' earthquakes—those with the largest magnitudes, $m \geq M$. Our goal is to predict them by analysing the whole sequence.

2.2 Premonitory seismicity patterns and prediction algorithm

We consider the earthquake precursors called *premonitory seismicity patterns.* These are the features of an earthquake sequence that indicate the approach of a major earthquake. Such patterns emerge only after sufficient averaging of seismicity, overcoming its high complexity. To use them for prediction, we have to give them an unambiguous definition, quantitative and reproducible. Different patterns considered here are defined in a uniform way.

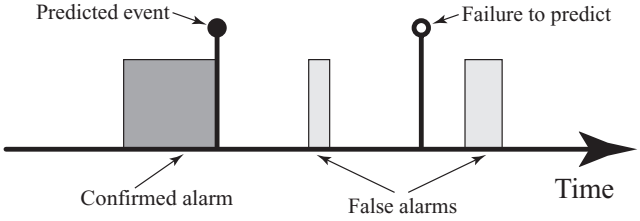

Figure 3. Outcomes of prediction.

(1) An earthquake sequence is described by a time function, $F(t)$, representing one of the robust averaged features of the sequence. Specific examples of such functions are given below.

(2) The emergence of a premonitory pattern is recognized by the condition

$$F(t) \geq C_F\,. \tag{2}$$

The threshold C_F is an adjustable parameter. It is usually defined to be a specified percentile of the function F.

The algorithm for prediction based on a single pattern is formulated as follows. An alarm is declared for a time period Δ_F whenever $F(t) \geq C_F$. The alarm is terminated after a major earthquake occurs or the time Δ_F expires, whichever comes first. The former case is called a *confirmed prediction* ('success'), while the latter is called a *false alarm*. A *failure to predict* emerges when a major earthquake occurs outside an alarm period (Fig. 3). In many prediction algorithms, an alarm is declared when certain combinations of premonitory patterns emerge (Keilis-Borok 1996; Gabrielov *et al.* 1986; Keilis-Borok & Shebalin 1999).

3 PERFORMANCE OF SINGLE PRECURSORS

We look for precursors in the same synthetic earthquake sequence, produced by the CC model described in the Appendices, as was analysed in Gabrielov *et al.* (2000). The sequence was generated by the model with seven levels, with the upper four

shown in Fig. 1. The numerical parameters used are given in Table 1. The complete sequence is shown in Fig. 2, while the Gutenberg–Richter relation for this sequence is given in Fig. 4.

The targets of prediction are 25 major earthquakes with magnitude $m=7$, the strongest possible in the model. Premonitory patterns are formed by earthquakes with smaller magnitudes, ranging from 6 down to 1.

We consider here three basic types of premonitory patterns. They reflect a premonitory increase of the following integral characteristics of seismicity:

(1) clustering of earthquakes in space and time (see Section 3.1);
(2) overall intensity of the sequence of earthquake flow (see Section 3.2); and
(3) correlation distances between the earthquakes (see Section 3.3).

Patterns of the first two types were established mainly by the analysis of observations and are used in the intermediate-term earthquake prediction algorithms [see Keilis-Borok (1999) and Keilis-Borok & Shebalin (1999) and references therein]. They precede a strong earthquake by a few years.

Patterns of the third type have been found just recently in the CC model (see Gabrielov *et al.* 2000), although they were hypothesized in Keilis-Borok (1994, 1996). They have yet to be validated by observations. Each pattern was defined separately for different magnitude ranges. Altogether, we analyse a set of 17 precursors related to the three characteristics of seismicity mentioned above as well as to different magnitude ranges.

Each precursor was used for prediction according to the scheme described above. An alarm was declared for $\Delta_F=10$ time units, the same for all precursors.

Table 1. Values of the parameters used in the computations.

γ	$\tilde{a}$	C	q	s	ε	λ	L	n
0.2	27.2	0.9	1.096	1.03	0.1	3.0	3.4	2

3.1 Premonitory clustering

3.1.1 Definition

Premonitory clustering is depicted by the precursor B, also called a 'burst of aftershocks' (Keilis-Borok *et al.* 1980). It is defined as a main shock with a large number of aftershocks, i.e.

$$B_m(t_k|s) \geq C_B\,,$$

where we have introduced the subscript m to indicate the magnitude of the main shock. We consider this precursor separately for individual values of m from 3 to 6.

In predicting real earthquakes, only the immediate aftershocks are counted in B, with $s=2$ days, while the whole aftershocks sequence may be much longer—a year or more. This is the first premonitory seismicity pattern for which statistical significance was established (Molchan *et al.* 1990; Keilis-Borok 1999).

Prediction by this pattern is illustrated in Fig. 5. Panel (a) shows the fragment of the earthquake sequence in the dimensionless time interval from 700 to 850. It contains one major earthquake, i.e. $m=7$, and nine main shocks with $m=5$. Panel (b) shows the values $B_5(t_k|0.05)$. Taking $C_B=4$, we obtain four alarms indicated by shaded intervals of the standard duration $\Delta_B=10$. One of them, the darkest one, is a confirmed alarm,

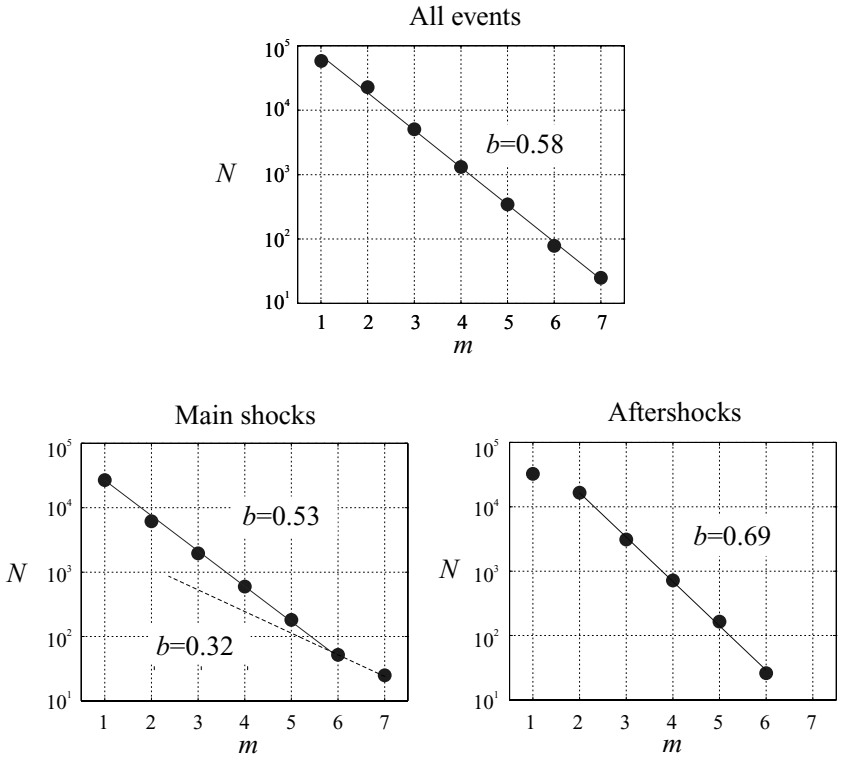

Figure 4. Energy distribution function, $\log_{10} N=a-bm$, where N is the number of events with magnitude m. Note that the magnitude is given discrete integer values from 1 to 7.

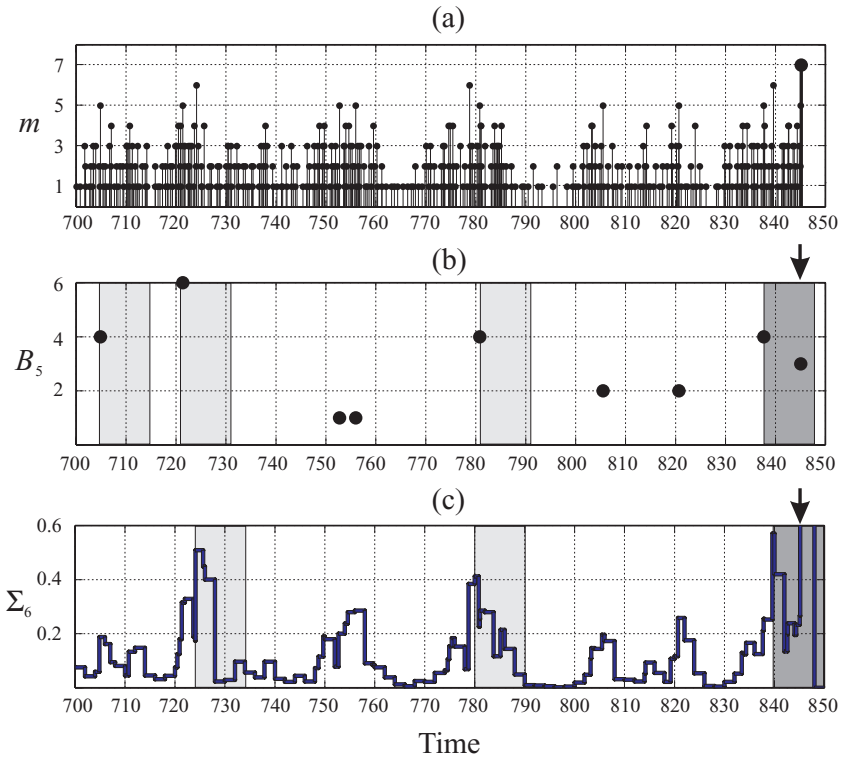

Figure 5. Emergence of premonitory patterns: a case history. This figure shows the time interval 700–850 preceding a major earthquake, $m=7$. The shaded time intervals correspond to alarms. The darkest interval is a confirmed alarm. Arrows indicate the time when a strong earthquake occurred. (a) The earthquake sequence; (b) the function $B_5(t_k, 0.05)$; (c) the function $\Sigma_6(t, 2)$.

during which a major earthquake occurred, while the other three are false alarms. The quality of a prediction algorithm, that is, the success-to-failure score, depends on the threshold C_B.

3.1.2 *Error diagram*

Figs 5(a) and (b) show the trade-off between confirmed predictions and errors. This trade-off depends on the adjustable parameters of a prediction algorithm. In this case, by raising C_B we would reduce the number of alarms but increase the number of failures to predict. On the other hand, by raising Δ we will increase the duration of alarms but may reduce the number of failures to predict, etc.

A prediction method and the evaluation of its performance make sense *only* if the success and error scores are insensitive to the variation of adjustable parameters such as C_F, Δ, the total duration of alarms, etc. That brings us to the *error diagram*—a pivotal element of any prediction algorithm—that was introduced to earthquake prediction research by Molchan (1990). The diagram shows the relative scores of successes and errors for different choices of adjustable parameters. Such a diagram for the pattern B_5 is shown in Fig. 6(a), which we now explain.

Prediction relates to a specified time interval T. During that time interval, N strong events occurred and N_f of them were not predicted. The number of declared alarms is A, with A_f of them being false alarms, and the total duration of alarms is D. Empty time intervals between the cycles—that is, time intervals lacking seismicity—are not counted in T. The right-hand plot shows the trade-off between the relative duration of alarms, $\tau=D/T$, and the rate of failures to predict, $n=N_f/N$. The diagonal, $n+\tau=1$ (the bold line), corresponds to a random binomial prediction—at each step in time the alarm is declared with some probability p and not declared with probability $q=1-p$. The left-hand plot shows the trade-off between the rate of false alarms, $f=A_f/A$, and n. Different points correspond to different thresholds C_B, varying from 3 at the lowest point to 9 at the highest point.

It is seen that, with the highest threshold in Fig. 6(a), the total duration of alarms, τ, is only 1 per cent of the time considered but there are 24 failures to predict ($n=24/25=0.96$) and about 65 per cent are false alarms. With the lowest threshold, we have $\tau=20$ per cent but no failures to predict and 70 per cent false alarms. Prediction with the other values of m from 3 to 6 gives similar results. Choosing for prediction a threshold in the middle range (4 to 5), we have $\tau=10$–15 per cent, $n=10$–40 per cent and $f=60$–65 per cent. For advance prediction of real earthquakes, the typical score is close to $n=\tau=30$ or 40 per cent, so that a diagram such as Fig. 6(a) would be quite satisfactory. Variation of other adjustable parameters, say Δ or s, may be explored in the same way but this is beyond the scope of the present study.

3.2 Premonitory rise of seismic activity

This phenomenon is depicted by the following two functions defined in a sliding time window $(t-s, t)$: $N_m(t|s)$, which is the number of main shocks of magnitude m, and

$$\Sigma_m(t|s)=\sum S_i(t|s)\,.$$

Here S_i is the area of the ith earthquake source; the summation is taken over all earthquakes with magnitudes from 1 to m. Note that the value of each function is attributed to the end of the window so we do not use information from the future.

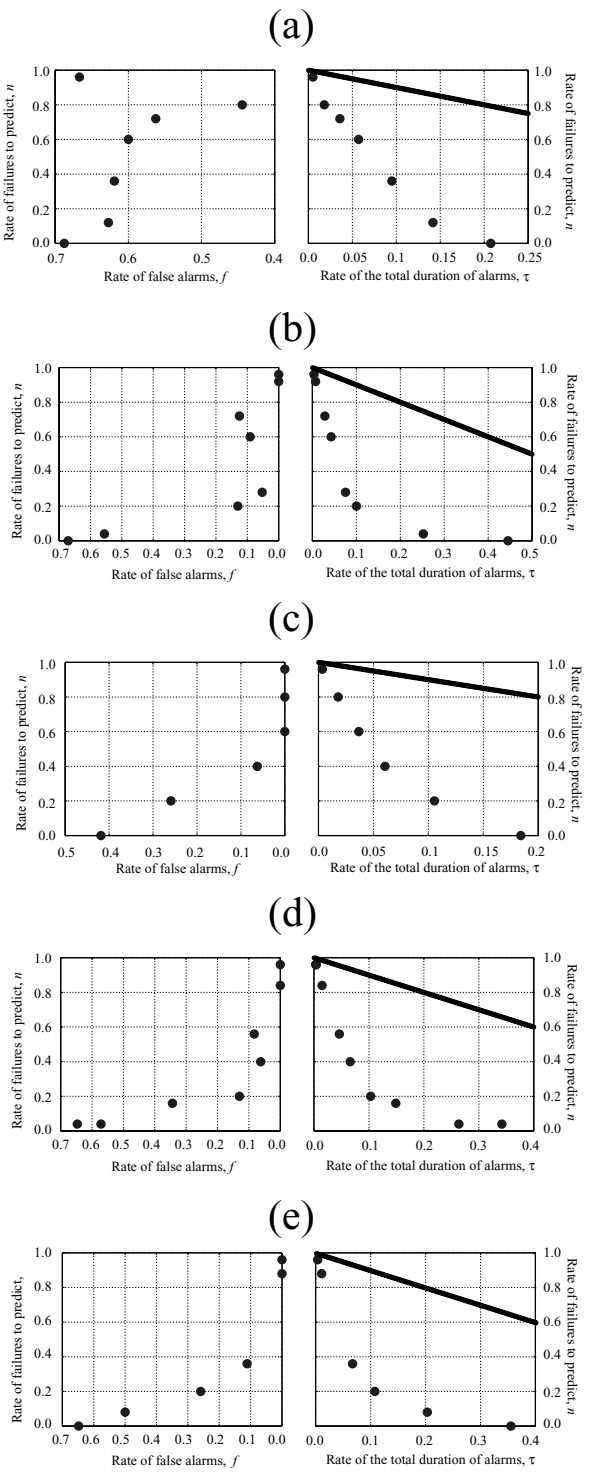

Figure 6. Error diagrams for (a) $B_5(t|0.05)$, (b) $N_2(t|2)$, (c) $\Sigma_6(t|2)$, (d) $R(t|0.1, 2)$ and (e) $A(t)$. See text for explanation.

In the analysis of observations, S_i is coarsely estimated from the earthquake magnitude. For synthetic seismicity, we assume that $S_i = 3^{m-\bar{m}}$, where $\bar{m}$ is the index of the top level (see Fig. 1) and m is the magnitude of the ith earthquake.

Precursors N_m were defined separately for each magnitude m from 1 to 6. Precursors Σ_m were defined for events of magnitudes within the range [1, m], with m varying from 2 to 6. As above, the premonitory patterns are defined by conditions $N \geq C_N$ and $\Sigma \geq C_\Sigma$. Error diagrams for prediction with these patterns are given in Figs 6(b) and (c). Comparing panels (b) and (c), we see that precursor Σ_m gives a slightly better prediction.

Fig. 5 reveals an intriguing correlation between precursors B_5, depicting clustering, and Σ_6, depicting activity. Fig. 5(c) shows the function $\Sigma_6(t|2)$ and alarms obtained with the threshold $C_\Sigma = 0.4$. The observed increase in Σ_6 corresponds to main shocks of middle magnitude 5 by definition. However, the fact that the heights of the peaks are strongly correlated with the number of immediate aftershocks is surprising. As a consequence, we observe in the interval shown that three alarms produced by pattern Σ_6 nearly coincide with three out of the four alarms produced by pattern B_5. A similar correlation was established by analysis of observed patterns B and Σ in California and several regions of the world (Keilis-Borok *et al.* 1980).

3.3 Premonitory rise of correlation distance in space

This phenomenon was first identified in the CC model (Gabrielov *et al.* 2000), although it was hypothesized previously in Keilis-Borok (1999) and Bowman *et al.* (1998). Importantly, Turcotte *et al.* (2000) and Bowman *et al.* (1998), more qualitatively, proposed the analogy between seismicity prior to a large earthquake and critical phase transitions studied in statistical physics, where the correlation length reaches the system size as the system approaches criticality (Wilson 1979). It is depicted by two functions described below.

3.3.1 *Pattern* ROC *('range of correlation')*

This precursor was defined in Gabrielov *et al.* (2000) on the synthetic sequence of events of magnitude 2. Let r be the pairwise (ultrametric) distance between elements of the model, counted along the tree's branches. [The word 'ultrametric' (Rammal *et al.* 1986) has now emerged in physics and mathematics to describe distances measured in a given tree and has some special mathematical properties. In particular, distance is determined by counting the number of nodes encountered in making a connection between any two points.] For elements of the second level in the seven-level model, r may assume an integer value from 0 to 5. We consider the function $R(t|\delta, s)$—the number of pairs of main shocks that occurred within a time interval δ from each other and at the maximal distance $r = 5$ between them. The pairs are counted within a sliding window of length $s > \delta$ in order to produce a modest degree of averaging. The pattern ROC is defined by the condition $R \geq C_R$. Error diagrams for prediction with this pattern are given in Fig. 6(d).

3.3.2 *Pattern* Accord

Let us determine the function $\Sigma_6(t|s)$ separately for the three major branches of the model that descend from the elements of the second highest level, $m = 6$. We define $A(t)$ as the number of branches where these functions *simultaneously* exceed a common threshold C_A. Accord describes a state of heightened activity in several adjoining branches. An elevated value of

Σ_6, on the other hand, could be due to major activity in a single branch or more moderate activity distributed over several branches. Accord represents our coarse measure of correlation between seismicity in these branches. Obviously, $A(t)$ may assume the integer values from 0 to 3. The premonitory pattern Accord is defined by the condition $A \geq 2$.

Error diagrams for prediction with this pattern are given in Fig. 6(e). There is a clear similarity with the diagram for ROC. This supports our hypothesis that both patterns reflect the same underlying phenomenon, the increase of the correlation distance between earthquakes.

3.4 Relation to definitions used in analysis of observations

The functions B_m, Σ_m and N_m are defined here in the same way as in the intermediate-term prediction algorithms developed by analysis of observations [see Keilis-Borok (1999) and Gabrielov *et al.* (1986) and references therein]. They were used in combination with other functions, while Σ and B were also used independently of the others. Premonitory patterns based on these functions have been validated by statistically significant earthquake prediction (Molchan *et al.* 1990; Kossobokov *et al.* 1999; Vorobieva 1999).

The pattern ROC is close to that introduced by Prozoroff (1975) for a long-term prediction of the location at which a strong earthquake is expected. The function A was first introduced in Gabrielov *et al.* (2000) in the analysis of the CC model. The scheme of the prediction algorithm is the same as for observed seismicity (see Section 2.2).

4 COLLECTIVE PERFORMANCE OF PRECURSORS

In the previous section, we considered predictions based on individual premonitory patterns, taken one at a time. Each pattern was applied independently in different magnitude ranges. In Figs 7, 8 and 9 we juxtapose the predictions by all 17 precursors considered. They are naturally divided into four groups: **B**, **N**, **Σ** and **R**. The names of the first three groups are self-explanatory; group **R** consists of the patterns ROC and Accord.

Figs 7 and 8 demonstrate the collective performance of all precursors. The top panels show, in separate boxes, the emergence of precursors before each of 25 major earthquakes in the synthetic sequence. The right edge of each box is the onset of a major earthquake. A time interval of three units is shown in each box.

The bottom panels in Figs 7 and 8 show the alarms determined during the time periods when strong earthquakes did not occur; those are the false alarms. Vertical lines show the moments of events with magnitude $m=6$. Evidently, $m=6$ events are associated with most of the false alarms.

Each row in Figs 7 and 8 shows the track record of a single precursor. Shaded areas show the alarms determined by the precursor. Values of m indicate the magnitude range in which a precursor is determined. Recall that precursors of the group **N** are determined separately for each magnitude m from 1 to 6. Precursors of the group **Σ** are determined separately for each magnitude interval [1, 2], [1, 3], [1, 6] and [4, 6]. The group **B** consists of a single precursor B for each magnitude m of the main shocks from 3 to 6.

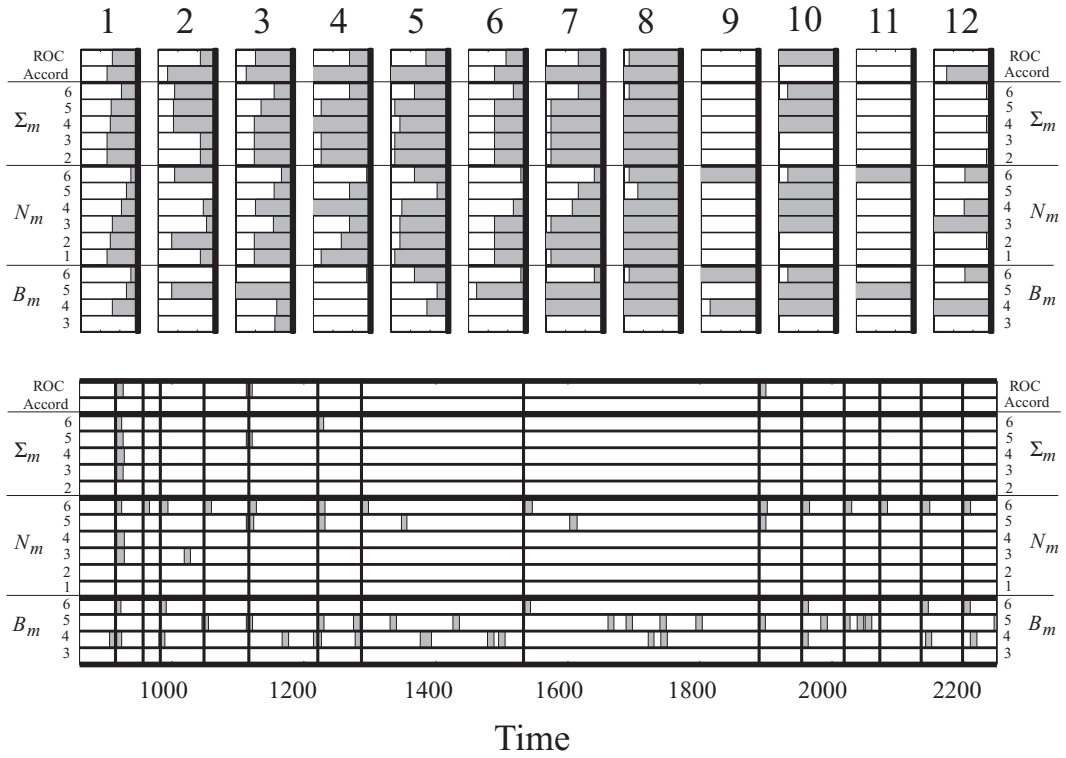

Figure 7. Collective performance of single premonitory patterns prior to major events 1–12. The figure juxtaposes alarms generated by all 17 precursors considered. The top panel shows confirmed alarms within the time interval of three units prior to strong earthquakes. The bottom panel shows false alarms. Details are given in the text.

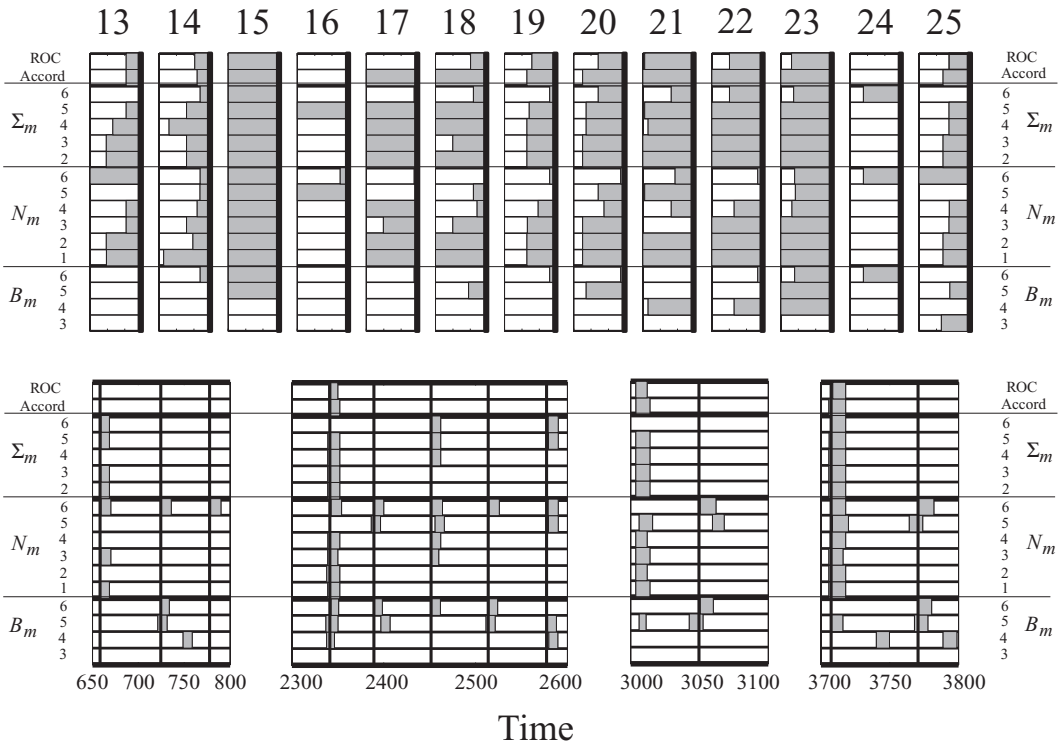

Figure 8. Collective performance of single premonitory patterns prior to major events 13–25. See caption to Fig. 7 for details.

It is seen that precursors B_m produce many false alarms. This fact is reflected in the error diagram shown in Fig. 6(a). The rate of false alarms for the precursor B_5 is about 60 per cent for all the variants considered.

Fig. 9 demonstrates the collective performance of each group of precursors. The top panel indicates whether a group predicts an event or not. We regard an event as predicted by a group if it is predicted by two or more single precursors from this group. Shaded boxes indicate events predicted by this rule. The bottom panel shows false alarms. Again, they are strongly associated with events of magnitude 6, shown by vertical lines.

The following inferences seem to deserve special attention.

(1) The emergence of precursors is highly correlated: almost all alarms are clearly grouped and act simultaneously. As seen from Figs 7 and 8, an isolated single alarm is a rare event. The lead times between the start of an alarm and a major event are correlated too. All the lead times prior to some major events, e.g. the eighth or 15th, are long, and they all are short prior to the other events, e.g. first or 19th. The correlation persists even for precursors reflecting such different phenomena as the clustering and the rise of activity. This correlation is emphasized by the similarity of the error diagrams (Fig. 6).

(2) Although the emergence of the major earthquakes follows a very simple 'seismic cycle' scenario, predictions are not trivial. For example, we have the following persisting errors: the failure to predict the major earthquakes 9, 11, 16 and 24, and the false alarms at times $t=660$, 2340, 3010 and 3710 (see Figs 7 and 8).

(3) Comparing these inferences with Fig. 2, we observe the following:

(i) failures to predict are characteristic for the first major earthquake in a cyclic regime of the sequence (major events 9, 11, 16 and 24);

(ii) the last major earthquake in a cyclic regime is preceded by most of the precursors, and the lead times in this case are unusually high (events 8, 15 and 23); and

(iii) false alarms usually occur at the end of cyclical regimes—they cover the interval where the next strong earthquake would occur unless the seismicity switched to a non-cyclical regime.

5 DISCUSSION

(1) The colliding cascade model is, we believe, the first model where such a broad set of precursors is reproduced.

(2) The data-adaptive design of the model alone guarantees good performance of the precursors N and Σ, while the performance of the precursors Accord and ROC can be qualitatively explained by that design. However, the success of the bursts of aftershocks, i.e. precursor B, and its correlation with Σ is not pre-determined as a consequence of our definition, which further supports the relevance of the model.

(3) This study suggests two new precursors, ROC and Accord, that depict an increase of the range of correlation in space for earthquake sequences. It seems worthwhile to explore their efficacy in real seismicity. A more general realization of the same phenomenon might be the spreading of the area manifesting premonitory patterns of seismicity. These precursors may be used in parallel with others, or they may help to identify false alarms obtained with other precursors.

(4) In nature, the occurrence of patterns of different types is observed to be correlated [Keilis-Borok *et al.* (1980) and Keilis-Borok & Shebalin (1999) and references therein]. Our model strongly reproduces that correlation. This hints at the possible existence of an underlying phenomenon—which may be not observable directly—that controls the model as a whole. Understanding this phenomenon is important for the further development of prediction algorithms.

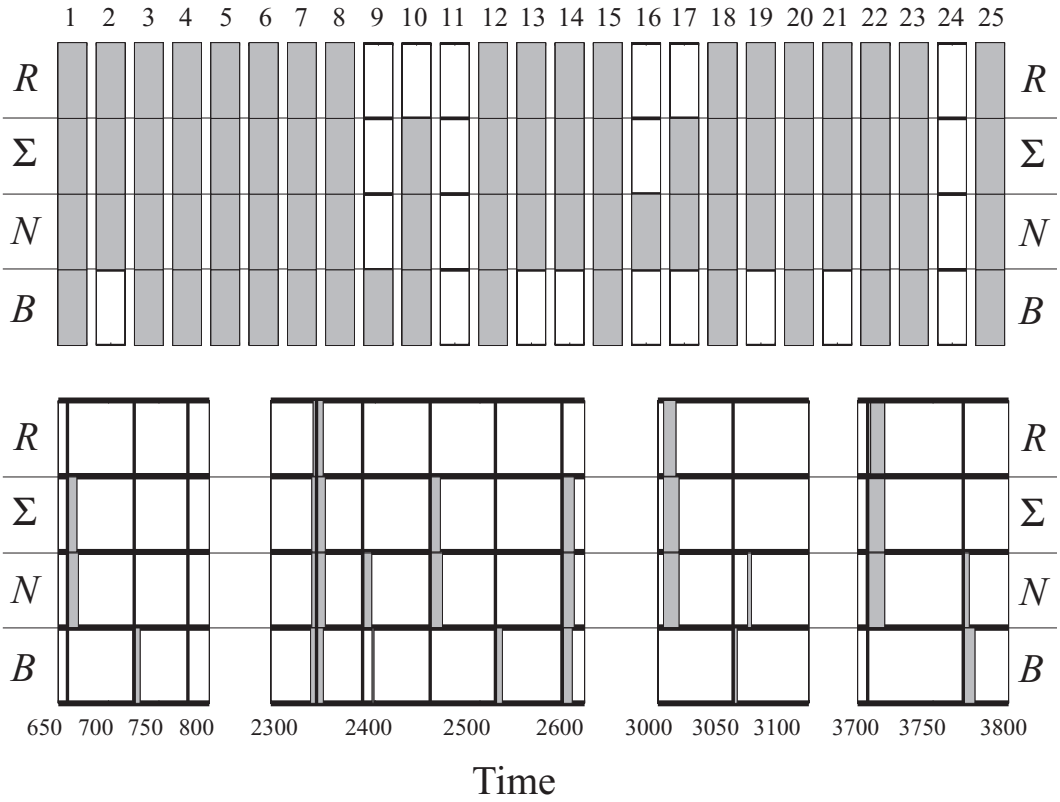

Figure 9. Collective performance of four types of premonitory patterns. The figure juxtaposes alarms generated by four different types of premonitory patterns. The top panel indicates whether the strong earthquake was predicted or not. The bottom panel shows false alarms. Details are given in the text.

(5) Many possibilities opened by the CC model remain untapped. These include:

(i) exploration of the three additional types of premonitory phenomena that have been previously hypothesized in Keilis-Borok (1996)—irregularity of sequences of earthquakes, response to excitation and decrease of dimensionality; and

(ii) more compact definition of the precursors set. Other possibilities of this kind are discussed in our previous paper (Gabrielov *et al.* 2000).

(6) Colliding cascades are not specific to seismicity, nor even to a more general phenomenon of the multiple fracturing in solids. The CC model probably exhibits regularities that are common in a wide class of complex hierarchical systems. It appears worthwhile to explore the application of this model to such systems.

ACKNOWLEDGMENTS

This study was partly supported by grants from the International Science and Technology Center (Project 1293-99) and the Italian Ministry for Foreign Affairs, by a subcontract with Cornell University, Geological Sciences, under grant EAR-9804859 from the National Science Foundation and administered by the CRDF, and by NSF grant ATM95-23787. We wish to thank our two external referees, Barbara Romanowicz and Donald Turcotte, for their insightful suggestions.

REFERENCES

Allègre, C.J., Le Mouel, J.L. & Provost, A., 1982. Scaling rules in rock fracture and possible implications for earthquake prediction, *Nature,* **297,** 47–49.

Bak, P., Chen, K. & Tang, C., 1992. A forest-fire model and some thoughts on turbulence, *Phys. Lett. A,* **147,** 297–300.

Barenblatt, G.I., 1982. *Similarity, Self-Similarity and Intermediate Asymptotics,* Consultants Bureau, New York.

Batchelor, G.K., 1959. *The Theory of Homogeneous Turbulence,* Cambridge University Press, Cambridge.

Blanter, E.M., Narteau, C., Shnirman, M.G. & Le Mouël, J.-L., 1999. Up and down cascade in a dynamo model: spontaneous symmetry breaking, *Phys. Rev. E,* **59,** 5112–5123.

Bowman, D.D., Ouillon, G., Sammis, C.G., Sornette, A. & Sornette, D., 1998. An observational test of the critical earthquake concept, *J. geophys. Res.,* **103,** 24 359–24 372.

Burridge, R. & Knopoff, L., 1967. Model and theoretical seismicity, *Bull. seism. Soc. Am.,* **57,** 341–371.

Drossel, B. & Schwabl, F., 1992. Self-organized criticality in a forest-fire model, *Phys. Rev. Lett.,* **69,** 1629–1632.

Gabrielov, A. & Newman, W.I., 1994. Seismicity modeling and earthquake prediction: a review, in *Nonlinear Dynamics and Predictability of Geophysical Phenomena,* pp. 7–13, eds Newman, W.I., Gabrielov, A. & Turcotte, D.L., AGU, Washington.

Gabrielov, A.M. *et al*, 1986. *Algorithms for Long-term Earthquake Prediction,* International School for Research Oriented to Earthquake Prediction, Lima, Peru.

Gabrielov, A., Newman, W.I. & Turcotte, D.L., 1999. An exactly soluble hierarchical clustering model: inverse cascades, self-similarity and scaling, *Phys. Rev. E,* **60,** 5293–5300.

Gabrielov, A., Keilis-Borok, V., Zaliapin, I. & Newman, W.I., 2000. Critical transitions in colliding cascades, *Phys. Rev. E,* **62,** 237–249.

Keilis-Borok, V.I. (ed.), 1990. Intermediate-term earthquake prediction: models, algorithms, worldwide tests, *Phys. Earth planet. Inter.,* **61**, special issue.

Keilis-Borok, V.I., 1994. Symptoms of instability in a system of earthquake-prone faults, *Physica D,* **77,** 193–199.

Keilis-Borok, V., 1996. Intermediate-term earthquake prediction, *Proc. Nat. Acad. Sci. USA,* **93,** 3748–3755.

Keilis-Borok, V.I. & Shebalin, P.N. (eds), 1999. Dynamics of lithosphere and earthquake prediction, *Phys. Earth planet. Inter.,* **111**, special issue.

Keilis-Borok, V.I., Knopoff, L. & Rotwain, I.M., 1980. Bursts of aftershocks, long-term precursors of strong earthquakes, *Nature,* **283,** 258–263.

Knopoff, L. & Newman, W.I., 1983. Crack fusion as a model for repetitive seismicity, *Pure appl. Geophys.,* **121,** 495–510.

Kolmogoroff, A.N., 1941. The local structure of turbulence in an incompressible viscous fluid for very large Reynolds number, *Doklady Akademii Nauk SSSR,* **30,** 299–303.

Kolmogoroff, A.N., 1941. On degeneration (decay) of isotropic turbulence in an incompressible viscous fluid, *Doklady Akademii Nauk SSSR,* **31,** 538–540.

Kossobokov, V.G., Romashkova, L.L., Keilis-Borok, V.I. & Healy, J.H., 1999. Testing earthquake prediction algorithms: statistically significant advance prediction of the largest earthquakes in the Circum-Pacific, 1992–1997, *Phys. Earth planet. Inter.,* **111,** 187–196.

Kraichnan, R.H. & Montgomery, D., 1980. Two-dimensional turbulence, *Rep. Prog. Phys.,* **43,** 547–619.

Malamud, B.D., Morein, G. & Turcotte, D.L., 1998. Forest fires: an example of self-organized critical behavior, *Science,* **281,** 1840–1842.

Molchan, G.M., 1990. Strategies in strong earthquake prediction, *Phys. Earth planet. Inter.,* **61,** 84–98.

Molchan, G.M., Dmitrieva, O.E., Rotwain, I.M. & Dewey, J., 1990. Statistical analysis of the results of earthquake prediction, *Phys. Earth planet. Inter.,* **61,** 128–139.

Narkunskaya, G.S. & Shnirman, M.G., 1990. Hierarchical model of defect development and seismicity, *Phys. Earth planet. Inter.,* **61,** 84–98.

Newman, W.I. & Knopoff, L., 1982. Crack fusion dynamics: a model for large earthquakes, *Geophys. Res. Lett.,* **9,** 735–738.

Newman, W.I. & Knopoff, L., 1983. A model for repetitive cycles of large earthquakes, *Geophys. Res. Lett.,* **10,** 305–308.

Newman, W.I. & Knopoff, L., 1989. Scale invariance in brittle fracture and the dynamics of crack fusion, *Int. J. Fracture,* **43,** 19–24.

Newman, W.I., Gabrielov, A. & Turcotte, D.L. (eds), 1994. *Nonlinear Dynamics and Predictability of Geophysical Phenomena,* Geophys. Monographs Ser. 83, AGU, Washington, DC.

Newman, W.I., Turcotte, D.L. & Gabrielov, A., 1995. Log-periodic behavior of a hierarchical failure model with applications to precursory seismic activation, *Phys. Rev. E,* **52,** 4827–4835.

Press, F. & Allen, C., 1995. Pattern of seismic release in the southern California region, *J. geophys. Res.,* **100,** 6421–6430.

Prozoroff, A.G., 1975. Variations of seismic activity related to locations of strong earthquakes, *Vychislitel'naya Seismologiya,* **8,** 71–72 (in Russian).

Rammal, R., Toulous, G. & Virasoro, M.A., 1986. Ultrametricity for physicists, *Rev. Mod. Phys.,* **58,** 765–788.

Romanowicz, B., 1993. Spatiotemporal patterns in the energy-release of great earthquakes, *Science,* **260,** 1923–1926.

Shnirman, M.G. & Blanter, E.M., 1999. Mixed hierarchical model of seismicity: scaling and prediction, *Phys. Earth planet. Inter.,* **111,** 295–304.

Tennekes, H. & Lumley, J.L., 1972. *A First Course in Turbulence,* MIT Press, Cambridge.

Turcotte, D.L., 1997. *Fractals and Chaos in Geology and Geophysics*, 2nd edn, Cambridge University Press, Cambridge.

Turcotte, D.L., Malamud, B.D., Morein, G. & Newman, W.I., 1999. An inverse cascade model for self-organized criticality, *Physica A,* **268,** 629–643.

Turcotte, D.L., Newman, W.I. & Gabrielov, A., 2000. A statistical physics approach to earthquakes, in *Geocomplexity and the Physics of Earthquakes*, pp. 83–96, eds Rundle, J.B., Turcotte, D.L. & Klein, W., AGU, Washington.

Vorobieva, I.A., 1999. Prediction of a subsequent large earthquake, *Phys. Earth planet. Inter.,* **111,** 197–206.

Wilson, K.G., 1979. Problems in physics with many scales of length, *Sci. Am.,* **241,** 140–157.

APPENDIX A: STRUCTURE OF THE MODEL

We consider a dynamical system acting on a ternary tree shown in Fig. 1. The nodes of the tree are called the *elements* of the system, and each element has its own *index*, consisting of two numbers, $i=(m|g)$. Here, m is the level where an element is situated and is enumerated from the bottom to the top of the hierarchy. The second integer, g, identifies the position of an element within its level m, counting from left to right, i.e. from 1 to $3^{\bar{m}-m}$, where $\bar{m}$ identifies the top level in the hierarchy. The indexing of elements is illustrated in Fig. 1. It is convenient to describe the taxonomy of this system using the imagery of a family tree. The top element $(\bar{m}|1)$ has three 'children'—the elements $(\bar{m}-1|1)$, $(\bar{m}-1|2)$ and $(\bar{m}-1|3)$. They are referred to as 'siblings', while the element $(\bar{m}|1)$ identifies their 'parent'. For example, the elements $(\bar{m}-2|4)$, $(\bar{m}-2|5)$ and $(\bar{m}-2|6)$ are the children of the parent element $(\bar{m}-1|2)$ and the siblings of each other. Conceptually, this structure is similar to that of a wavelet, where the complementary dimensions, crudely the position and (the logarithm of) the wavelength, have a direct physical meaning and significance.

APPENDIX B: DYNAMICS OF THE MODEL

The behavior of an arbitrary element i is described by two functions, namely a continuous positive-valued function, $\sigma_i(t)$, and a Boolean function, $f_i(t)$. We think of $\sigma_i(t)$ as the 'load' supported by an element and of $f_i(t)$ as its 'state'. An element i is 'whole' or intact when $f_i(t)=0$, and 'broken' or failed when $f_i(t)=1$. The direct cascade of loading is described by the set of functions $\{\sigma_i(t)\}$, while the inverse cascade of fracturing is described by the set of functions $\{f_i(t)\}$. The dynamics of the system is described by interaction of direct and inverse cascades. The functions $\sigma_i(t)$ satisfy a system of ordinary differential equations with the right sides depending upon the functions $\{f_i(t)\}$. The functions $f_i(t)$ change their values according to certain logical rules or conditions that depend upon $\sigma_i(t)$ and $\{f_i(t)\}$. Like almost all models of seismicity (Gabrielov & Newman 1994), this model is non-Markovian since the changes made to the states of each of its elements depend on the history of the system.

B1 Loading

The loading of elements is determined by the following system of ordinary differential equations:

$$\dot{\sigma}_i(t)=U_i(t)-W_i(t)\,. \tag{B1}$$

Here

$$W_i(t)=\begin{cases}\dfrac{\beta\sigma_i(t)}{\theta-\sigma_i(t)}\,, & \text{if } f_i(t)=0\\ \alpha\sigma_i(t)\,, & \text{if } f_i(t)=1\end{cases}$$

and

$$U_i(t)=CW_{\rm p}(t)+\frac{1-C}{2}\,W_{\rm s1}(t)+\frac{1-C}{2}\,W_{\rm s2}(t)\,,\quad 0\le C\le 1\,,$$

for all i except the top element

$$U_{\rm top}(t)=v\,.$$

The parameters β, θ, α, C are positive. The subscript p refers to the parent of the ith element, while subscripts s1 and s2 refer to its two siblings. The load supported by an intact element can never exceed the *critical threshold* θ. In the stationary case, when the time derivatives in eq. (B1) vanish, we have the steady-state solutions

$$\sigma^{\rm w}_{i,{\rm ss}}\equiv\frac{\theta v}{v+\beta} \tag{B2}$$

for a whole element i, and

$$\sigma^{\rm b}_{i,{\rm ss}}\equiv\frac{v}{\alpha} \tag{B3}$$

for a broken one. We assume that at time $t=0$ all elements are intact, i.e. $f_i(0)=0$, and support no load, i.e. $\sigma_i(0)=0$. As given by eq. (B1), the load is added to the hierarchical system through the top element and is subsequently redistributed among all other elements in the tree. Since all dynamical equations are symmetric with respect to the siblings' indices (i, s1, s2), all of the elements on any level retain the same load until at least one element fails.

B2 Failure

A whole element $i\neq(\bar{m}|1)$ fails when the following condition is satisfied:

$$\sigma_i(t)\ge\theta\; q^{-[f_{\rm c1}(t)+f_{\rm c2}(t)+f_{\rm c3}(t)]}\; s^{-[f_{\rm s1}(t)+f_{\rm s2}(t)]}\,,\quad q\ge 1\,,\quad s\ge 1\,. \tag{B4}$$

Here, the subscripts c1, c2 and c3 refer to the three children of the ith element, while s1 and s2 refer to its two siblings. The exponents of q and of s indicate the number of broken children and siblings respectively. If all children and siblings of the ith element are intact then this condition reduces to

$$\sigma_i(t)\ge\theta\,.$$

If some of the siblings or children are broken, the ith element is weakened, that is, the threshold for failure is reduced. The parameters q and s in eq. (B4) quantitatively determine this weakening. Eq. (B4), which describes the top element, reduces to

$$\sigma_{\rm top}(t)\ge\theta\; q^{-[f_{\rm c1}(t)+f_{\rm c2}(t)+f_{\rm c3}(t)]}$$

due to the absence of siblings. As we have mentioned above, the load applied to an intact element can never exceed θ. Therefore, an element cannot fail until at least one of its siblings or children fails. Accordingly, the failures propagate upwards and thereby form an inverse cascade. At the bottom level of the tree, where the elements have no children, we introduce random failures with a rate proportional to the intensity of the direct cascade. This mimics 'juvenile cracking' in earthquake phenomenology. Let t_s be the time when the load of an element rises close to the stationary value, $\sigma_i(t)\ge\sigma^{\rm w}_{i,{\rm ss}}-\varepsilon$, for ε small and positive. This element fails at a later time, $t_{\rm s}+\chi$, where χ is a random variable, distributed exponentially with a decay time λ. This randomness ensures that the dynamics of our model shows a degree of inhomogeneity in spite of the symmetry mentioned above.

B3 Healing

In order to ensure the perpetual operation of our system, we introduce the effect of 'healing', that is, the restoration to an unbroken state of a previously broken element. Otherwise, the system will cease to function once all elements have failed. We assume that a broken element heals when the following two conditions hold during the ensuing exponentially distributed time interval with a decay time L. At least n children of the ith element are intact, and

$$\sigma_i(t)<\theta\; q^{-[f_{\rm c1}(t)+f_{\rm c2}(t)+f_{\rm c3}(t)]}\; s^{-[f_{\rm s1}(t)+f_{\rm s2}(t)]}\,. \tag{B5}$$

Finally, at the bottom level we replace (B5) by

$$\sigma_i(t)<\theta\,. \tag{B6}$$